ORIGINAL RESEARCH

Mixed Valvular Disease Following Transcatheter Aortic Valve Replacement: Quantification and Systematic Differentiation Using Clinical Measurements and Image-Based Patient-Specific In Silico Modeling

Zahra Keshavarz-Motamed, PhD; Seyedvahid Khodaei, MS; Farhad Rikhtegar Nezami, PhD; Junedh M. Amrute, BS; Suk Joon Lee, BS; Jonathan Brown, BS; Eyal Ben-Assa, MD; Tamara Garcia Camarero, MD; Javier Ruano Calvo, MD; Stephanie Sellers, MD; Philipp Blanke, MD; Jonathon Leipsic, MD; Jose M. de la Torre Hernandez, MD, PhD; Elazer R. Edelman, MD, PhD

***Background*—**Mixed valvular disease (MVD), mitral regurgitation (MR) from pre-existing disease in conjunction with paravalvular leak (PVL) following transcatheter aortic valve replacement (TAVR), is one of the most important stimuli for left ventricle (LV) dysfunction, associated with cardiac mortality. Despite the prevalence of MVD, the quantitative understanding of the interplay between pre-existing MVD, PVL, LV, and post-TAVR recovery is meager.

***Methods and Results*—**We quantified the effects of MVD on valvular-ventricular hemodynamics using an image-based patient-specific computational framework in 72 MVD patients. Doppler pressure was reduced by TAVR (mean, 77%; N=72; $P<0.05$), but it was not always accompanied by improvements in LV workload. TAVR had no effect on LV workload in 22 patients, and LV workload post-TAVR significantly rose in 32 other patients. TAVR reduced LV workload in only 18 patients (25%). PVL significantly alters LV flow and increases shear stress on transcatheter aortic valve leaflets. It interacts with mitral inflow and elevates shear stresses on mitral valve and is one of the main contributors in worsening of MR post-TAVR. MR worsened in 32 patients post-TAVR and did not improve in 18 other patients.

***Conclusions*—**PVL limits the benefit of TAVR by increasing LV load and worsening of MR and heart failure. Post-TAVR, most MVD patients (75% of N=72; $P<0.05$) showed no improvements or even worsening of LV workload, whereas the majority of patients with PVL, but without that pre-existing MR condition (60% of N=48; $P<0.05$), showed improvements in LV workload. MR and its exacerbation by PVL may hinder the success of TAVR. **(*J Am Heart Assoc*. 2020;9:e015063. DOI: 10.1161/JAHA.119.015063.)**

Key Words: left ventricle hemodynamics • mitral regurgitation • mixed valvular disease • paravalvular leak • transcatheter aortic valve replacement

Transcatheter aortic valve replacement (TAVR) is an emerging minimally invasive intervention for patients with aortic stenosis (AS) *across a broad risk spectrum.*[1] TAVR is increasingly used in lower-risk (moderate valvular disease and/or young) patients as well. Although TAVR has provided positive outcomes and has remarkably reduced the mortality rate, there are risks associated with TAVR procedures. Many patients experience significant improvements after TAVR intervention, but in many others, the situation worsens and pre-existing valvular diseases transform to even

From the Department of Mechanical Engineering, McMaster University, Hamilton, Ontario, Canada (Z.K.-M., S.K.); Institute for Medical Engineering and Science, Massachusetts Institute of Technology, Cambridge, MA (Z.K.-M., F.R.N., J.M.A., J.B., E.B.-A., J.M.d.l.T.H., E.R.E.); Harvard Medical School, Boston, MA (S.J.L.); Division of Biology and Biological Engineering, California Institute of Technology, Pasadena, CA (J.M.A.); Cardiology Division, Massachusetts General Hospital (E.B.-A.) and Cardiovascular Division, Brigham and Women's Hospital (E.R.E.); Hospital Universitario Marques de Valdecilla, IDIVAL, Santander, Spain (T.G.C., J.R.C., J.M.d.l.T.H.); St. Paul's Hospital, Vancouver, British Columbia, Canada (S.S., P.B., J.L.); Department of Radiology, University of British Columbia, Vancouver, British Columbia, Canada (S.S., P.B., J.L.).

An accompanying Data S1 is available at https://www.ahajournals.org/doi/suppl/10.1161/JAHA.119.015063

Correspondence to: Zahra Keshavarz-Motamed, PhD, Department of Mechanical Engineering, McMaster University, 1280 Main St W, John Hodgins Engineering Building, Room JHE-310, Hamilton, Ontario, Canada, L8S 4L7. E-mail: motamedz@mcmaster.ca

Received October 23, 2019; accepted January 9, 2020.

Clinical Perspective

What Is New?

- Valvular disease is a complex disease that also depends on the dictates of the left ventricle and the arterial system.
- We developed a computational mechanics framework based on and correlated with clinically measured hemodynamic metrics and imaging in patients to noninvasively quantify the effect of: (1) mixed valvular disease on the left ventricle workload (global hemodynamics) and (2) mixed valvular disease on the flow structures (local hemodynamics) in the left ventricle and investigated the correlation of hemodynamics parameters with clinical metrics in both pre- and postintervention states.

What Are the Clinical Implications?

- Paravalvular leak limits the benefit of transcatheter aortic valve replacement: It may increase left ventricle load, may potentially worsen mitral regurgitation, and worsens heart failure. Mitral regurgitation and its possible exacerbation by paravalvular leak will likely play an important hindering role in the success of transcatheter aortic valve replacement.
- This represents an important finding, especially considering the expansion of transcatheter aortic valve replacement candidacy to lower-risk and/or young patients.
- Our findings suggest that beyond standard clinical indices for hemodynamic evaluation of the valvular disease, valvular and ventricular hemodynamics and their interactions should be quantified and considered for better management of patients with aortic valve disease.

more-extensive disease (eg worsened mitral regurgitation [MR] and heart failure).[2–4]

Despite recent improvements in the design of transcatheter heart valves and implantation techniques, paravalvular leak (PVL; leak around the prosthesis) remains a major complication and an independent predictor of short- and long-term mortality.[5,6] As Pibarot[7] noted, "Paravalvular regurgitation is considered the main Achilles' heel of transcatheter aortic valve replacement." Mild PVL occurs in 20% to 80% of patients, whereas moderate and severe PVL occur in 5% to 22% of them.[7–9]

Mixed valvular disease (MVD), mitral regurgitation (MR) from pre-existing disease in conjunction with PVL following TAVR, is one of the most important stimuli for left ventricle (LV) dysfunction resulting in congestive heart failure, associated with worsening cardiac mortality.[2,7,9–13] As indications and use of TAVR expand, we must advance our understanding of its interactions with diseases of other valves and the ventricular state.[2,7,10,13–15] However, despite the prevalence of MVD, the quantitative understanding of the interplay between pre-existing valvular pathologies, PVL, LV, and post-TAVR recovery is meager. This study was aimed to elucidate the relationship between MR, LV function, and TAVR.

"Cardiology is flow."[16] The main functions of the cardiovascular system are to transport, control, and maintain blood flow in the entire body. Abnormal fluid dynamics greatly alter this tranquil picture, leading to initiation and progression of disease[17]. These abnormalities are often manifested by disturbed flow, altered biomechanical forces, and, in some cases, an increase in heart workload. The hypothesis is increasingly appreciated that valvular disease is a complex disease that also depends on the dictates of the LV and arterial system.[18–21] There has thus been an emerging call by many for quantitative investigations of hemodynamics that take the interactive coupling of the valve, ventricle, and arterial system into account.[18–21]

In this study, we developed a Doppler-based, patient-specific, lumped-parameter modeling framework that takes interactions of the aortic valve, LV, and arterial system into account to investigate MVD and estimate LV workload noninvasively. We showed that effective quantification of MVD hinges on quantification of the load it imposes on the LV. We quantified the effect of MVD on LV workload (*global hemodynamics*) and investigated the correlation of LV workload with the metrics currently used in clinical practice in 72 MVD patients in both pre- and post-TAVR states. In addition to global hemodynamics, we provide a mechanistic fundamental understanding about the effect of MVD on the 3-dimensional flow structures in the LV and LV outflow tract (*local hemodynamics*). For local hemodynamics analysis, we developed a computational fluid mechanics and lumped-parameter modeling framework based on and correlated with clinically measured hemodynamic metrics and clinical images in both pre- and post-TAVR states.

Methods

Data Availability

The data and the code that support the findings of this study are available from the corresponding author upon request.

Study Population

We retrospectively and randomly selected 205 patients with severe AS who underwent TAVR from anonymized databases between 2013 and 2018 from the following institutions: St. Paul's Hospital (Vancouver, British Columbia, Canada; N=40); Massachusetts General Hospital (Boston, MA; N=40)[22]; and Hospital Universitario Marques de Valdecilla (IDIVAL, Spain; N=125). Selections were done by operators blinded to the objectives and contents of this study at each institution. Of

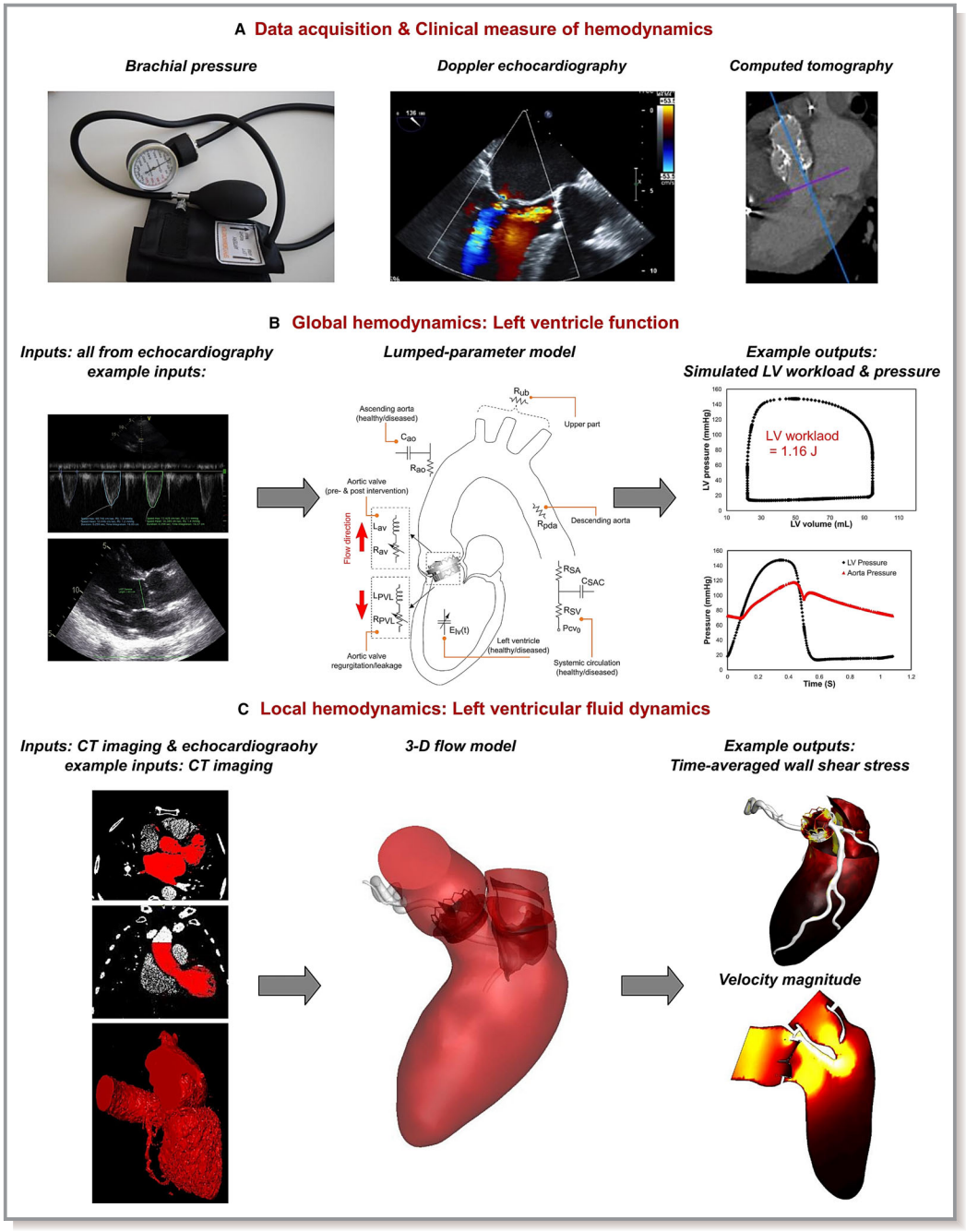

Figure 1. Left ventricular function and hemodynamics. (**A**) Data acquisition. We developed a computational mechanics framework based on noninvasive clinically measured hemodynamic metrics (brachial blood pressure and Doppler echocardiography measurements) and computed tomography imaging to estimate local and global hemodynamics. (**B**) Schematic diagram of lumped parameter model. Inputs of the lumped model were all obtained from Doppler echocardiography measurements. This model includes several submodels: left ventricle, aortic valve, aortic regurgitation, and systemic circulation. (**C**) Schematic diagram of 3D flow model. Inputs of the 3D flow model were obtained from CT and Doppler echocardiography. We used CT images from patients to reconstruct 3D geometries of the LV and valves. These 3D reconstructions were used for investigating hemodynamic using computational fluid dynamics. Moreover, imposing correct boundary conditions to the flow model is critical because the local flow dynamics is influenced by down- and upstream conditions. These data were obtained from a lumped parameter model (part B). C_{ao} indicates aortic compliance; C_{SAC}, systemic arteries and veins compliance; CT, computed tomography; 3D, 3-dimensional; E_{LV}, left ventricle elastance; L_{av}, aortic valve inductance; L_{PVL}, paravalvular leak inductance; LV, left ventricle; R_{ao}, aortic resistance; R_{av}, aortic valve resistance; R_{pda}, proximal descending aorta resistance; R_{PVL}, paravalvular leak resistance; R_{SA}, systemic arteries resistance; R_{SV}, systemic vein resistance; R_{ub}, upper body resistance.

Table 1. Baseline Clinical and Echocardiographic Characteristics

	AS Patients (n=72, Mean±SD)
Patient description	
Mean age, y	74.40±6.54
Female sex	(48%)
Mean weight, kg	71.71±13.92
Mean height, cm	161.86±10.13
Body surface area, m^2	1.77±0.16
Body mass index, kg/m^2	32.38±23.20
EuroScore II	7.04±7.68
STS mortality rate	6.62±5.33
Arterial hemodynamics	
Systolic arterial pressure, mm Hg	139.0±22.5
Diastolic arterial pressure, mm Hg	79.0±11.7
Aortic valve hemodynamics	
Stenotic aortic valve effective orifice area, cm^2	0.58±0.16
Stenotic aortic valve type	Tricuspid: 70; bicuspid: 2
Maximum aortic valve pressure gradient, mm Hg	84.50±21.32
Mean aortic valve pressure gradient, mm Hg	51.52±13.60
Left ventricle hemodynamics	
Ejection fraction, %	53.5±12.7
Stroke volume index, mL/m^2	45.7±11.5
Heart rate, bpm	71.0±11.5
Associated cardiovascular lesions	
Previous percutaneous coronary intervention	33%
Previous coronary artery bypass grafting	34%
Previous myocardial infarction	21%
Previous stroke	2%
Atrial fibrillation	29%
Cerebrovascular accident	9%
Peripheral vascular disease	29%
Hypertension	74%

AS indicates aortic stenosis; STS, Society of Thoracic Surgeons.

Table 2. Summarized Cardiovascular Parameters Used in the Lumped Parameter Modeling to Simulate All Cases

Description	Abbreviation	Value
COA and valve parameters		
Effective orifice area	EOA	From echocardiography data
Energy loss coefficient	E_LCo	$\frac{(EOA)A}{A-EOA}$ From echocardiography data
Variable resistance	R_{av} and R_{PVL}	$\frac{\rho}{2E_LCo^2}Q$
Inductance	L_{av} and L_{PVL}	$\frac{2\pi\rho}{\sqrt{E_LCo}}$
Systematic circulation parameters		
Aortic resistance	R_{ao}	0.05 mm Hg·s·mL^{-1}
Aortic compliance	C_{ao}	Initial value: 0.5 mL/mm Hg Adjust for each degree of hypertension (proximal COA compliance)
Systemic vein resistance	R_{SV}	0.05 mm Hg·s·mL^{-1}
Systemic arteries and veins compliance	C_{SAC}	Initial value: 2 mL/mm Hg Adjust for each degree of hypertension (systemic compliance)
Systemic arteries resistance (including arteries, arterioles and capillaries)	R_{SA}	0.8 mm Hg·s·mL^{-1} Adjust according to the calculated total systemic resistance
Proximal descending aorta resistance	R_{pda}	0.05 mm Hg·s·mL^{-1}
Upper body resistance	R_{ub}	Adjusted to have 15% of total flow rate in healthy case
Output condition		
Central venous pressure	P_{CV0}	4 mm Hg
Input condition		
Mitral valve mean flow rate	Q_{mv}	From echocardiography data
Other		
Constant blood density		1050 kg/m^3
Heart rate	HR	From echocardiography data
Duration of cardiac cycle	T	From echocardiography data

COA indicates coractation of the aorta.

these 205 patients, 72 had MVD (MR from pre-existing disease and PVL following TAVR). The protocol was reviewed and approved by the ethics committees of the institutions. Suitability and eligibility for receiving TAVR were determined by the local clinical team. Data were acquired at 2 time points: preprocedure and 90-day postprocedure. Valve type and size were planned before the procedure by the local clinical team according to preprocedural

echocardiographic, tomographic, and angiographic parameters. Procedural techniques were at the discretion of the local senior interventional cardiologists.

Doppler echocardiography

Doppler echocardiography data included raw images, and reports were collected preprocedure and at 90-day postprocedure. Echocardiograms and reports were reviewed and analyzed in a blinded fashion by 3 senior cardiologists using OsiriX imaging software (OsiriX version 8.0.2; Pixmeo, Bernex, Switzerland). The following metrics were measured: valve area, valve velocity, pressure gradient, stroke volume, cardiac output, and left ventricular outflow tract diameter, as recommended by the American Society of Echocardiography.

Data acquisition

Demographic and procedural data were collected from the TAVR database and patient medical records. Clinical outcome was evaluated using the New York Heart Association functional class and medical records, evaluated preprocedure and 90-day post-TAVR.

Statistical analysis

All results are expressed as mean±SD. Normal distribution was assessed with the Shapiro–Wilk test. Statistical analyses were performed using SigmaStat software (Version 3.1; Systat Software, Inc, San Jose, CA). The paired Student *t* test was used to detect any significant hemodynamic difference between pre- and post-TAVR conditions.

Numerical study

Global hemodynamics (LV workload). We developed a patient-specific, lumped-parameter model that considers interactions of the aortic valve, LV, and arterial system to estimate LV workload noninvasively (Figure 1; Tables 1 and 2) in both pre- and postintervention conditions. The model used a limited number of input parameters, all of which can be reliably obtained using Doppler echocardiography and a sphygmomanometer. Doppler echocardiography-based parameters (eg, stroke volume, heart rate, ejection time, ascending aorta area, aortic valve effective orifice area, and aortic regurgitation effective orifice area) were measured in the parasternal long axis, parasternal short axis, and apical 2-, 4-, and 5-chamber views of the heart.[22] Other input parameters of the model were systolic and diastolic blood pressures measured using a sphygmomanometer. Note that the proposed method does not need catheter data for estimating LV workload. The model and submodels have already been used and validated against in vivo cardiac catheterization (N=118) and in vivo magnetic resonance imaging data (N=57).[22–26] LV workload (global hemodynamics) was calculated in all 205 patients in both pre- and post-TAVR.

Local hemodynamics (blood flow dynamics). We developed a fluid-solid interaction and lumped parameter modeling framework to calculate 3-dimensional blood flow dynamics in the LV (Figure 1; Tables 1 and 2). Because computed tomography images have higher resolution than Doppler echocardiography data, they were used for 3-dimensional reconstruction of the LV for fluid-solid interaction calculations. In addition, as described above, the lumped parameter model in this framework used few input parameters, all of which can be measured using Doppler echocardiography and a sphygmomanometer. Because of the massive computational load, the blood flow inside the LV (local hemodynamics) was computed and analyzed in 28 of 72 patients with MVD.

Please refer to Data S1 for the details related to the numerical study.

Results

Clinical Measure of Hemodynamics: Doppler Echocardiography Pressure Gradients

Clinical assessment of AS for management and intervention decisions is currently performed based on the symptoms

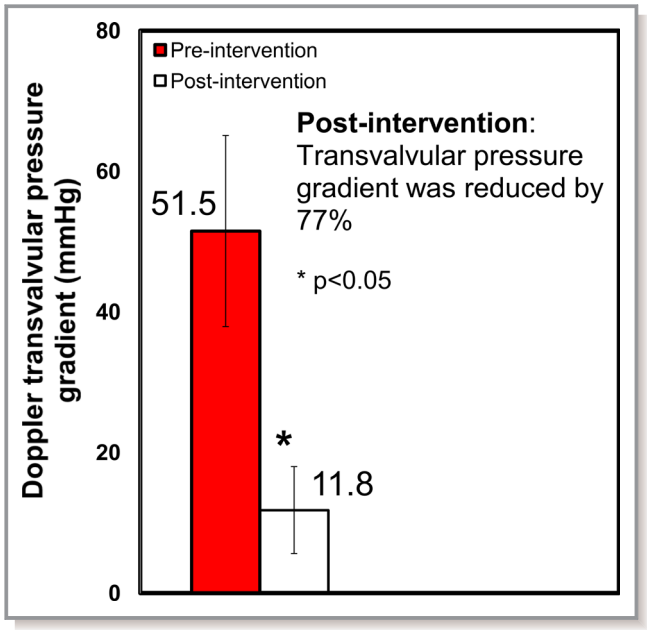

Figure 2. Changes in clinical Doppler echocardiography measurements in patients with MVD between baseline and 90 days post-TAVR (N=72). Mean Doppler gradient measured was reduced 77% by TAVR.

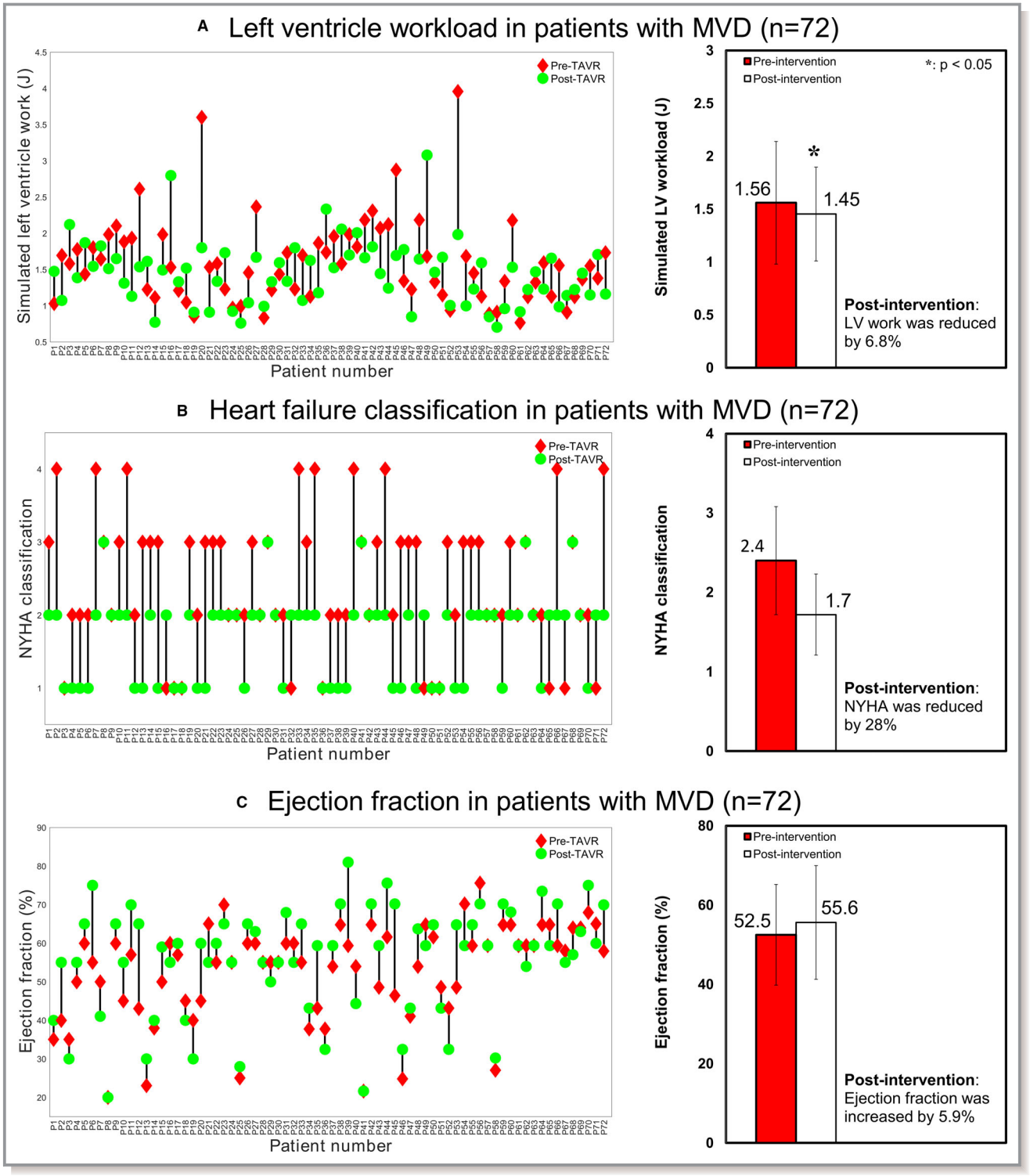

Figure 3. Changes in clinical assessments of LV and LV workloads in patients with MVD between baseline and 90 days post-TAVR (N=72). (**A**) LV workload. (**B**) Heart failure classification. (**C**) Ejection fraction. LV indicates left ventricle; MVD, mixed valvular disease; NYHA, New York heart association; TAVR, transcatheter aortic valve replacement.

and hemodynamics metrics that focus only on the aortic valve. Our Doppler echocardiography data showed (Figure 2) that the transvalvular pressure gradient in all patients with MVD (MR and PVL; Table 1) was universally significantly reduced by TAVR. Mean and maximum Doppler pressure gradients were reduced by 77% and 49%, respectively (N=72; $P<0.05$).

Hemodynamics: Left Ventricular Workload and Fluid Dynamics

LV workload (global hemodynamics)

Despite the universal reduction in the transvalvular pressure gradient (N=72; Figure 2), TAVR reduced the LV workload in only 18 of the 72 MVD patients (25%), as Figure 3A shows. In 22 of the MVD patients, LV workload was not significantly reduced (<5% reduction) post-TAVR, and in the other 32 patients, LV workload increased post-TAVR. Furthermore, reductions in transvalvular pressure gradient were not always accompanied by improvements in clinical metrics such as New York Heart Association heart failure classification (Figure 3B) and ejection fraction (Figure 3C). Pre-TAVR,

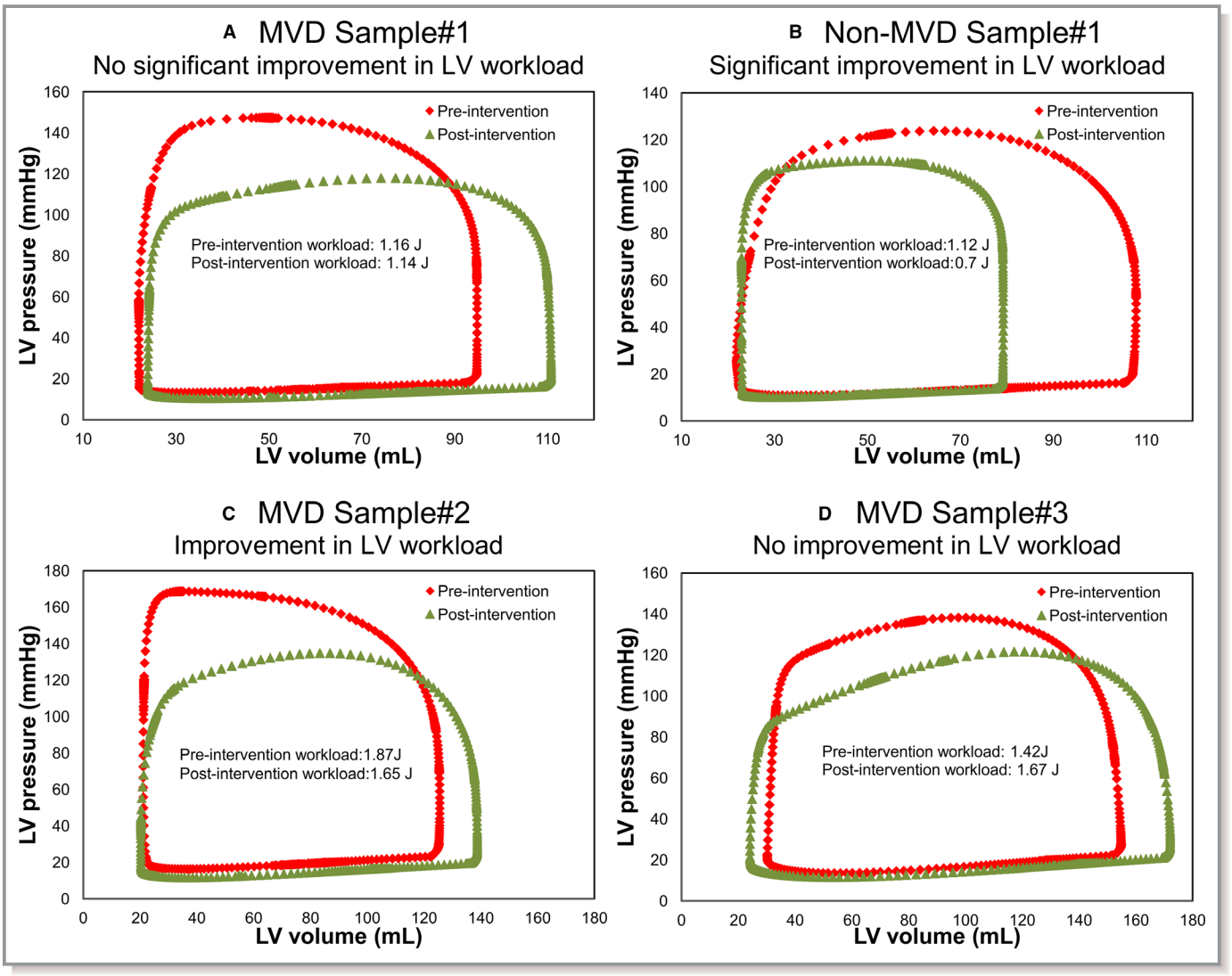

Figure 4. Examples of LV workloads in patients between baseline and 90 days post-TAVR. (**A**) MVD Sample#1: *pre-TAVR:* EF: 65%, brachial pressures: 65 to 130 mm Hg, aortic valve EOA: 0.66 cm^2, no AR, no MR, LV stroke volume: 72 mL; *post-TAVR*: EF: 60%, brachial pressures: 60 to 130 mm Hg, aortic valve EOA: 1.45 cm^2, mild PVL, mild MR, LV stroke volume: 80 mL. *LV workload did not improve by TAVR*. (**B**) Non-MVD Sample#1: *pre-TAVR:* EF: 58%, brachial pressures: 56 to 86 mm Hg, aortic valve EOA: 0.6 cm^2, mild-moderate AR, mild MR, LV stroke volume: 76 mL; *post-TAVR*: EF: 75%, brachial pressures: 70 to 123 mm Hg, aortic valve EOA: 1.1 cm^2, no PVL, no MR, LV stroke volume: 60 mL. *LV workload improved remarkably (38% reduction) by TAVR*. (**C**) MVD Sample#2: *pre-TAVR:* EF: 55%, brachial pressures: 74 to 180 mm Hg, aortic valve EOA: 1.95 cm^2, mild-moderate AR, mild-moderate MR, LV stroke volume: 87 mL; *post-TAVR*: EF: 65%, brachial pressures: 40 to 141 mm Hg, aortic valve EOA: 1.55 cm^2, mild PVL, mild-moderate MR, LV stroke volume: 103 mL. *LV workload slightly improved (12% reduction) by TAVR*. (**D**) MVD Sample#3: *pre-TAVR:* EF: 65%, brachial pressures: 75 to 141 mm Hg, aortic valve EOA: 1.4 cm^2, no AR, moderate MR, LV stroke volume: 85 mL; *post-TAVR*: EF: 65%, brachial pressures: 60 to 123 mm Hg, aortic valve EOA: 2.3 cm^2, mild-moderate PVL, moderate-severe MR, LV stroke volume: 100 mL. *LV workload did not improve by TAVR*. AR indicates aortic regurgitation; EF, ejection fraction; EOA, effective orifice area; LV, left ventricle; MR, mitral regurgitation; MVD, mixed valvular disease; PVL, paravalvular leakage; TAVR, transcatheter aortic valve replacement.

untreated AS increased the burden on the LV attributable to the augmented flow resistance, which caused an LV pressure overload. Although the flow resistance and consequently the LV pressure decreased greatly post-TAVR, the LV workload did not improve because PVL and MR contributed to a switch from a ventricular pressure overload to a ventricular volume overload. Figure 4 shows examples of LV pressure, volume, and workload in 4 patients who received TAVR: LV workload improved remarkably in Non-MVD Sample#1 (38% reduction), slightly improved in MVD Sample#2 (12% reduction), whereas it did not improve in MVD Samples#1 and 3.

LV fluid dynamics (local hemodynamics)

PVL following TAVR substantially alters vortical structure in the left ventricular outflow tract and LV, creating disturbed flow (Figures 5 through 7). The jets emerging from PVL orifices diverge within the LV. This unfavorable flow condition leads to high shear stresses (Figures 5 through 7) on transcatheter aortic valve and mitral valve leaflets (Figures 5 through 7; eg, peak time-averaged wall shear stress in patient #28 with MVD: on transcatheter aortic valve leaflets=14.4 Pa; on mitral valve leaflets=15.5 Pa; peak time-averaged wall shear stress in the same patient without PVL: on transcatheter aortic valve leaflets=0.8 Pa; on mitral valve leaflets=5.7 Pa). Moreover, PVL, characterized by multiple jets, enters the LV chamber, directly interacts with mitral inflow, hinders formation of normal fluid vortical structures in the LV, and may worsen the MR post-TAVR (eg, Figures 5 through 7). We observed similar flow characteristics in other patients with mild, moderate, and severe PVL. Interestingly, worsening of the average MR status post-TAVR (measured by clinical Doppler echocardiography) confirmed our above findings about the local hemodynamics (Figure 8A and 8B). We found in 72 MVD patients: (1) MR status was individually improved in only 21 patients (29% of MVD patients); on average: pre-TAVR, 2.4±0.5; post-TAVR, 1.2±0.45 (Figure 8C). The average of the LV workload was also improved

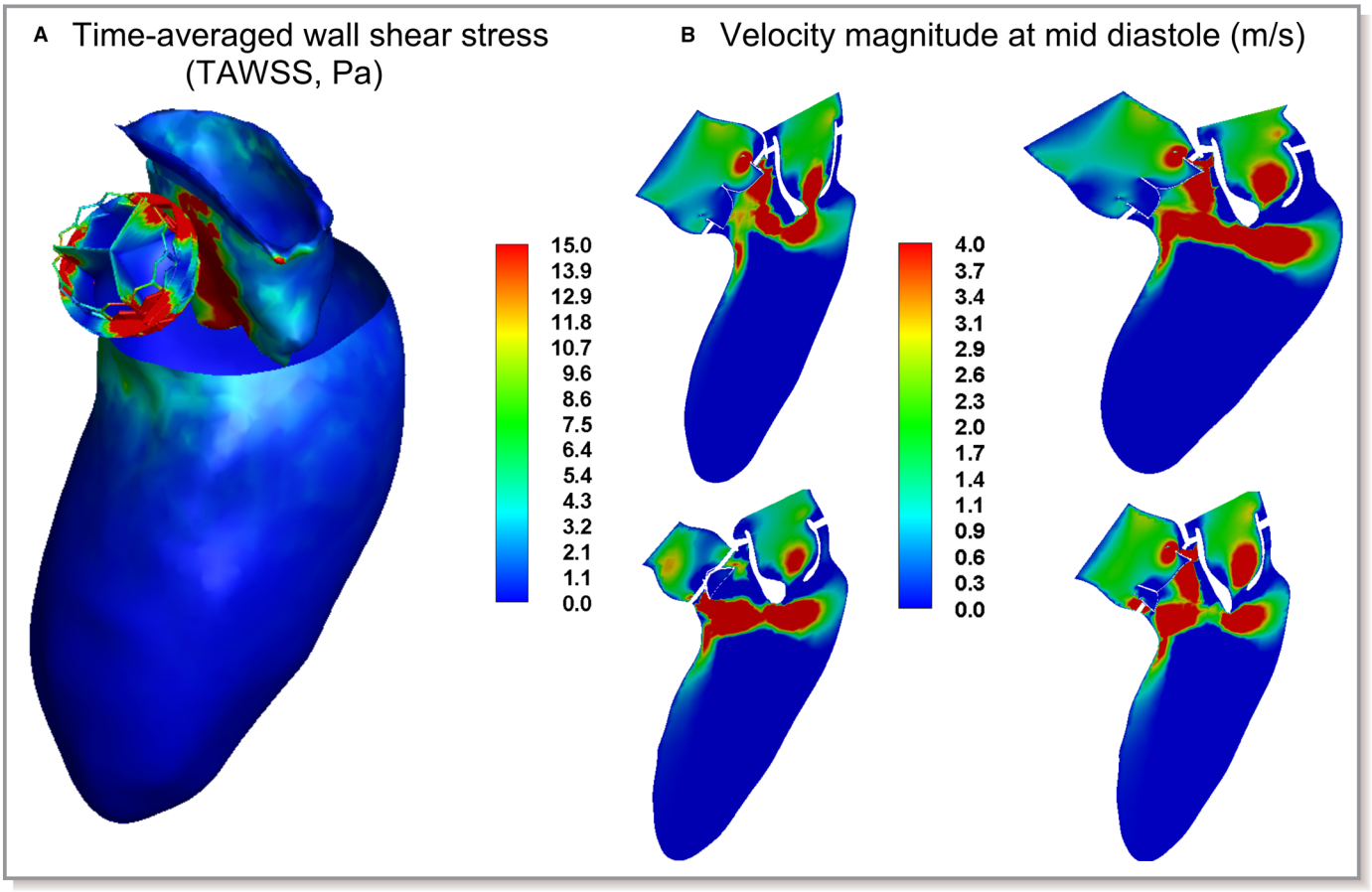

Figure 5. Flow modeling in an LV with moderate-to-severe PVL in patient #28. (**A**) Time-averaged wall shear stress (TAWSS) during diastole. Total shear stress exerted on the wall throughout was evaluated using the TAWSS, which was obtained as $\text{TAWSS} = \frac{1}{T}\int_0^T |\tau| dt$. Here, T and τ are the period and instantaneous wall shear stress, respectively. (**B**) Velocity magnitude at mid diastole in different planes passing PVL. In patient #28, PVL, characterized by 2 jets, enters the LV chamber, directly interacts with the mitral inflow, and may worsen the MR post-TAVR (MR status from Doppler echocardiography measurements: pre-TAVR, mild to moderate; post-TAVR, moderate to severe). This abnormal flow condition leads to high shear stresses on the mitral valve leaflets, LV wall, and TAV leaflets. LV indicates left ventricle; MR, mitral regurgitation; PVL, paravalvular leakage; TAV, transcatheter aortic valve; TAVR, transcatheter aortic valve replacement.

in this patient population (pre-TAVR, 1.99±0.55 J; post-TAVR, 1.37±0.29 J; 31% average decrease); (2) individual MR status became worse in 32 other MVD patients post-TAVR; on average: pre-TAVR, 1.15±0.38; post-TAVR, 2.25±0.40 (Figure 8D). The average of the LV workload was not improved in this patient population as well (pre-TAVR, 1.37±0.50 J; post-TAVR, 1.6±0.53 J; +17% average increase); and (3) individual MR status remained unchanged in 18 other MVD patients post-TAVR; on average: pre-TAVR, 1.66±0.48; post-TAVR, 1.66±0.48 (Figure 8E). The average of the LV workload was also not improved significantly in these patients (pre-TAVR, 1.45±0.51 J; post-TAVR, 1.31±0.36 J; 10% average decrease).

Figure 9 shows changes in LV workloads versus mitral valve effective regurgitant orifice area (measured by Doppler echocardiography) between baseline and 90-day post-TAVR in patients with MVD (N=72). In all panels of this figure, patients with negative changes in LV workload benefited from TAVR (shaded regions). Figure 9A suggests that, in some patients (quadrant IV), although TAVR worsened the mitral regurgitation condition, it still improved LV workload. Figure 9B

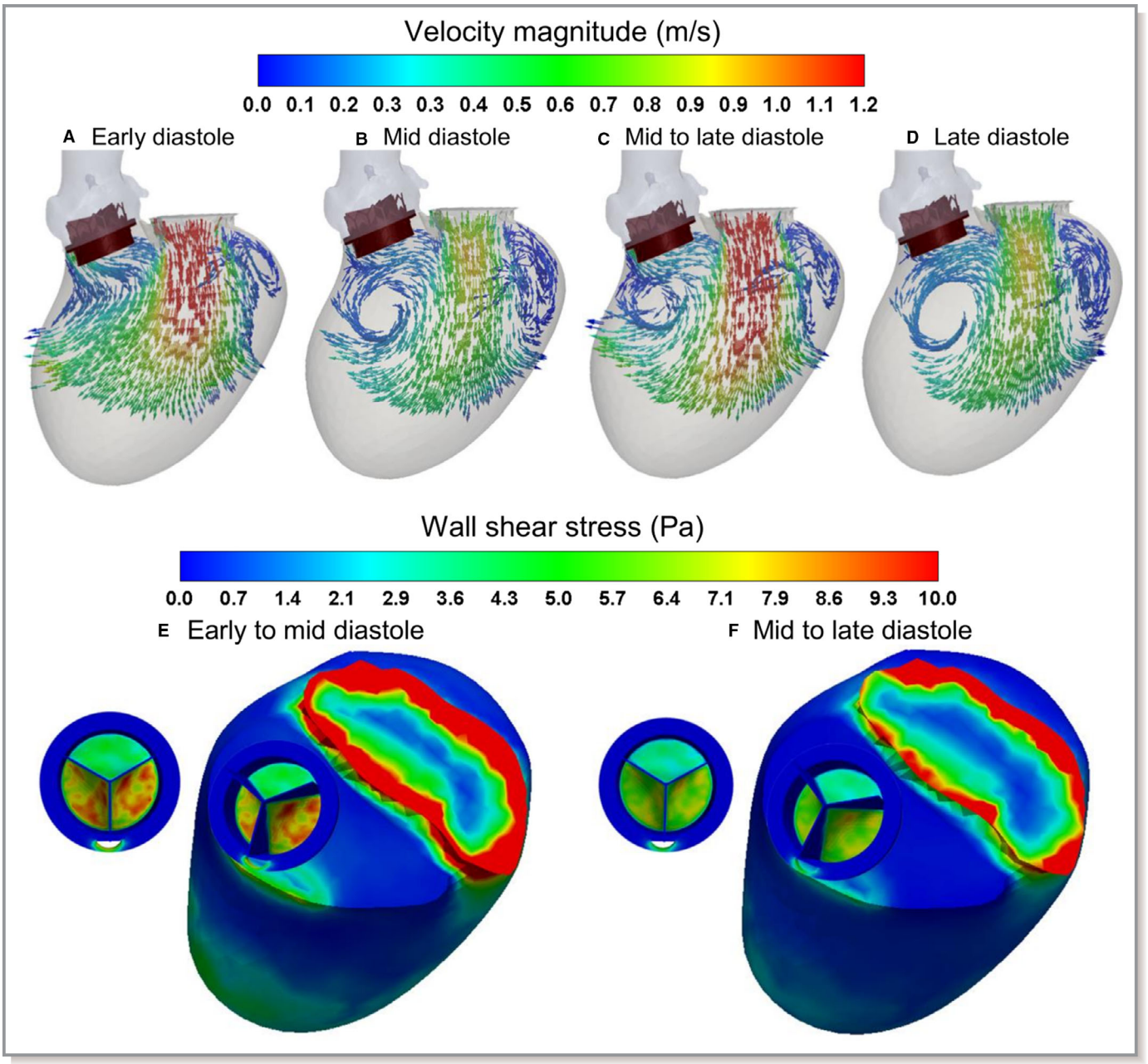

Figure 6. Flow modeling in an LV with mild-to-moderate PVL in patient #59. (**A**) Velocity vector during diastole. (**B**) Wall shear stress during diastole. In patient #59, PVL, described by 1 jet, interacts with the mitral inflow and may worsen the MR post-TAVR (MR status from Doppler echocardiography measurements: pre-TAVR, mild; post-TAVR, mild to moderate). LV indicates left ventricle; MR, mitral regurgitation; PVL, paravalvular leakage; TAVR, transcatheter aortic valve replacement.

suggests that all patients with pre-TAVR regurgitant mitral valve effective regurgitant orifice area >0.3 (moderate and worse) benefited from TAVR regardless of the conditions of other disease constituents. Interestingly, Figure 9C suggests that LV workload worsened in all patients who were found to have regurgitant mitral valve effective regurgitant orifice area >0.3 (moderate and worse) post-TAVR.

Discussion

In MVD, valvular (PVL and MR), and ventricular (eg, LV dysfunction and heart failure) diseases interact with one another, and these phenomena are independent predictors of short- and long-term mortality following TAVR. We showed that reduction of transvalvular pressure gradient does not predict outcome of TAVR because of the effects of the PVL on MR and LV hemodynamics. Given that the benefit of TAVR has been unequivocally shown, an important concern is how to address pathologies in other valves—at the same time, before or after TAVR procedure, and medically or mechanically. Our study brings mechanistic insight to address this increasingly common clinical dilemma.

In MVD Patients: Mitral Regurgitation May Be Exacerbated by Paravalvular Leak Post-TAVR

MR is a common entity in patients with AS—and perhaps it even arises from the long-term effects of pressure overload from the stenotic valve. Concomitant MR, left untreated at the time of TAVR, has been associated with increased all-cause

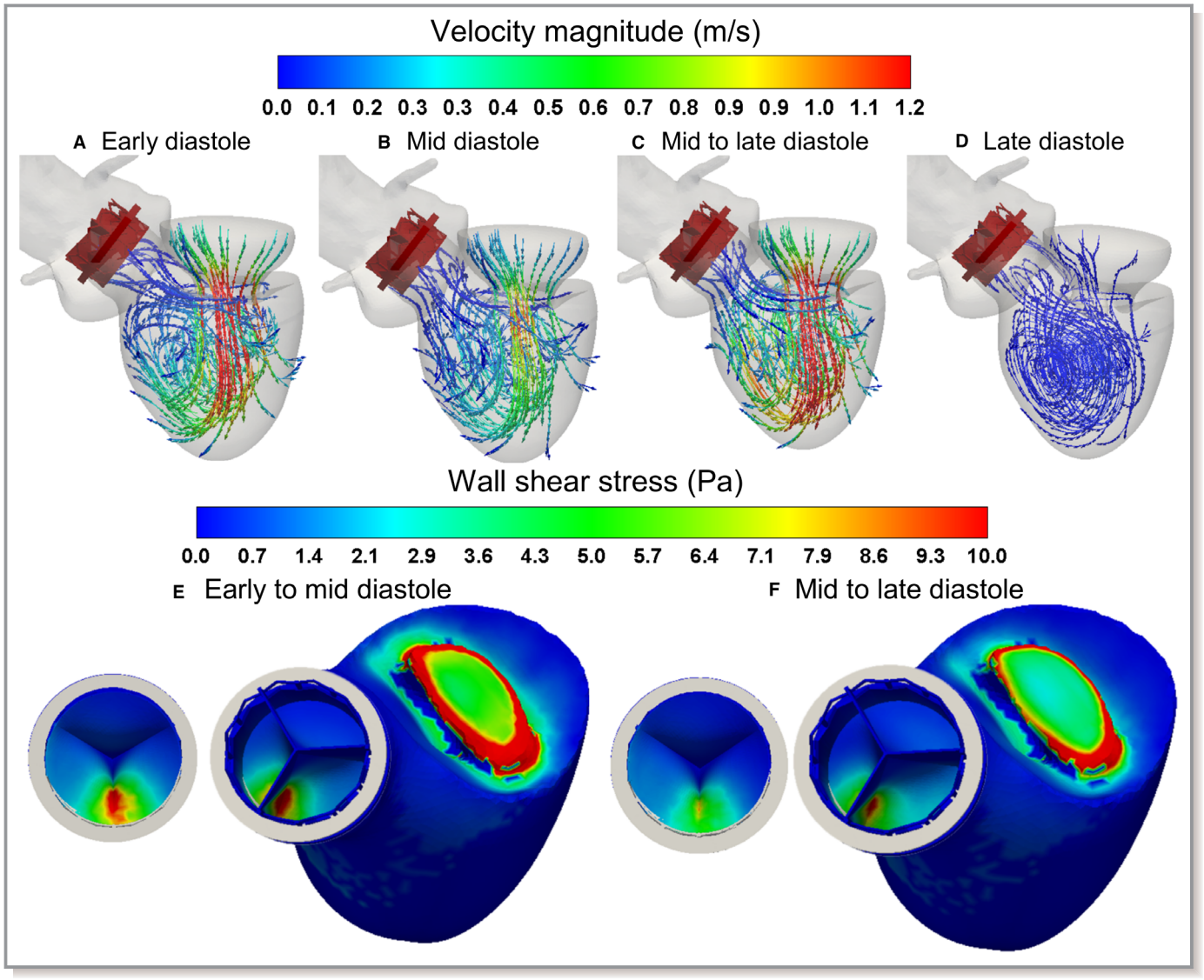

Figure 7. Flow modeling in an LV with mild PVL in patient #35. (**A**) Velocity vector during diastole. (**B**) Wall shear stress during diastole. In patient #35, PVL, defined by 1 jet, interacts loosely with the mitral inflow (MR status from Doppler echocardiography measurements: pre-TAVR: mild; post-TAVR: mild). LV indicates left ventricle; MR, mitral regurgitation; PVL, paravalvular leakage; TAVR, transcatheter aortic valve replacement.

mortality.[2,10–12] MR may increase patients' vulnerability because any complication leading to fluid dynamics or workload instability may rapidly decompensate the patient's hemodynamic status, leading to a refractory heart failure and shock. We are already aware that many patients experience a significant improvement in the MR post-TAVR, but, in many others, MR worsens.[2,10,12] Substantial MR was reported to increase early (in-hospital or 30-day) mortality post-TAVR.[27,28] It is crucial to identify patients in whom MR will not improve or will even progress post-TAVR.[29] In these patients, the increased risk of a double-valve procedure may be justified.

Pre-existing MR may be exacerbated by PVL

During filling of the healthy heart, the blood entering the LV through the mitral valve forms a vortex that minimizes energy dissipation and optimizes pumping efficiency.[30] The vortical structure in the LV is altered in the presence of valvular and ventricular diseases. In such cases, vortex dynamics become less synchronized with the heart contraction than the healthy vortex ring is, and other vortices may emerge and interact with one another.[30] In agreement with findings of Pibarot et al,[6] our results suggest that PVL, characterized by multiple jets, enters the LV and directly interacts with mitral inflow (eg, Figures 5 through 7) and worsens MR in MVD patients post-TAVR. These modeling findings were confirmed by our clinical Doppler echocardiography data (Figures 8 and 9): From 72 MVD patients, individual MR status worsened in 32 patients and remained unchanged in 18 others post-TAVR.

Additionally, we observed (Figures 5 through 7) that PVL leads to elevated shear stresses on mitral valve leaflets. This

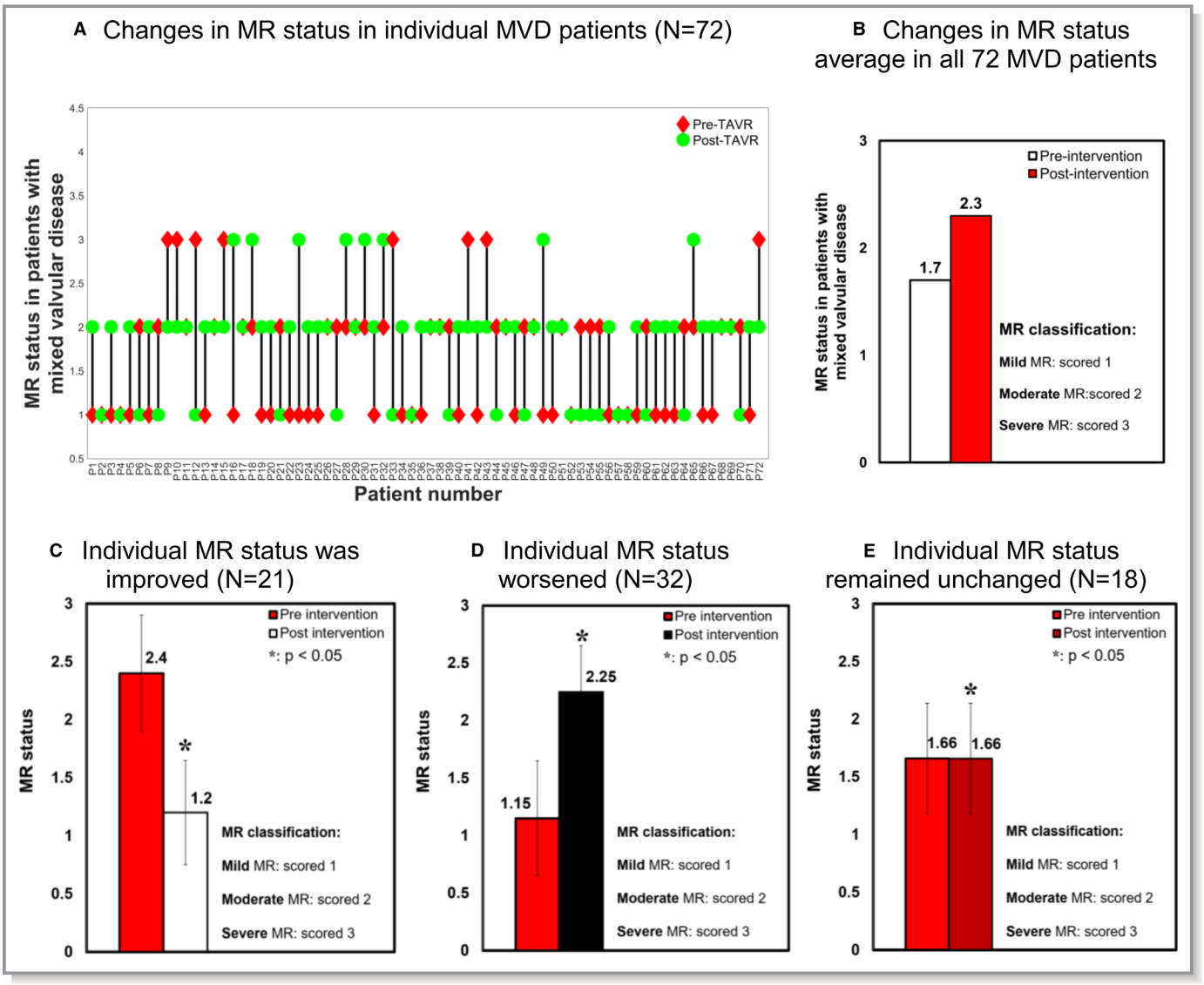

Figure 8. Changes in mitral regurgitation status in patients with MVD between baseline and 90 days post-TAVR (N=72). (**A**) In individual MVD patients. (**B**) Average in all 72 MVD patients. (**C**) Individual MR status was improved. (**D**) Individual MR status worsened. (**E**) Individual MR status remained unchanged. MR indicates mitral regurgitation; MVD, mixed valvular disease; TAVR, transcatheter aortic valve replacement.

can cause tissue inflammation, which can ultimately lead to mitral valve failure (34–37).

In Some MVD Patients: No Improvement in Left Ventricular Hemodynamics Post-TAVR

Some patients, who underwent TAVR, experienced a significant improvement in terms of pronounced reverse LV remodeling and less congestive heart failure symptoms. However, the situation in some other patients worsened. LV workload is an effective metric of LV load and clinical state[23,25,31] and represents the energy that the ventricle delivers to the blood during ejection plus the energy necessary to overcome the viscoelastic properties of the myocardium itself. LV workload is the integral of LV pressure and its volume change and was calculated as the area encompassed by the LV pressure-volume loop. Our results revealed that, pre-TAVR, AS increased the burden on the LV attributable to augmented flow

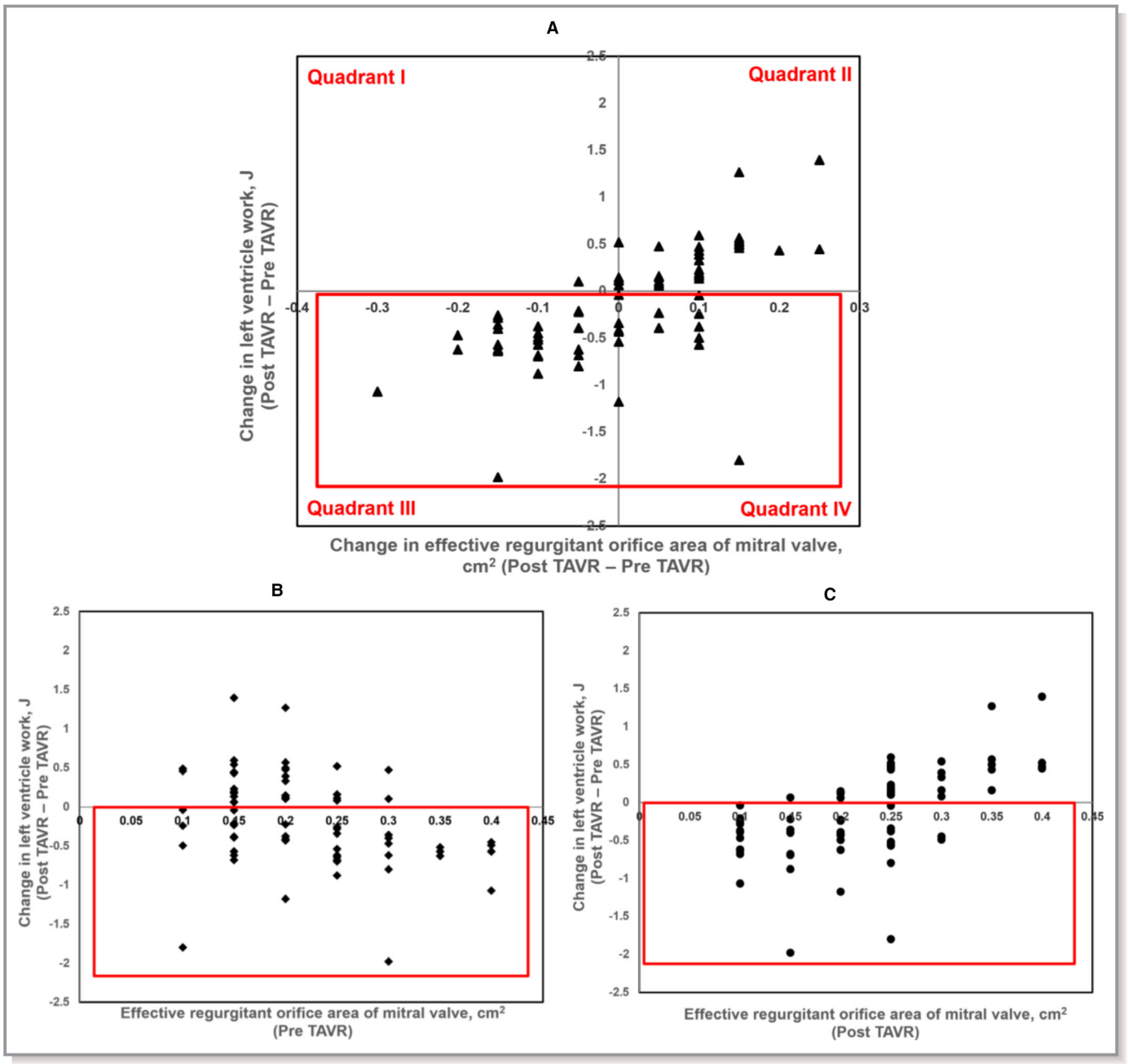

Figure 9. Changes in LV workloads vs mitral valve effective regurgitant orifice area in patients with MVD between baseline and 90 days post-TAVR (N=72). LV indicates left ventricle; MVD, mixed valvular disease; TAVR indicates transcatheter aortic valve replacement.

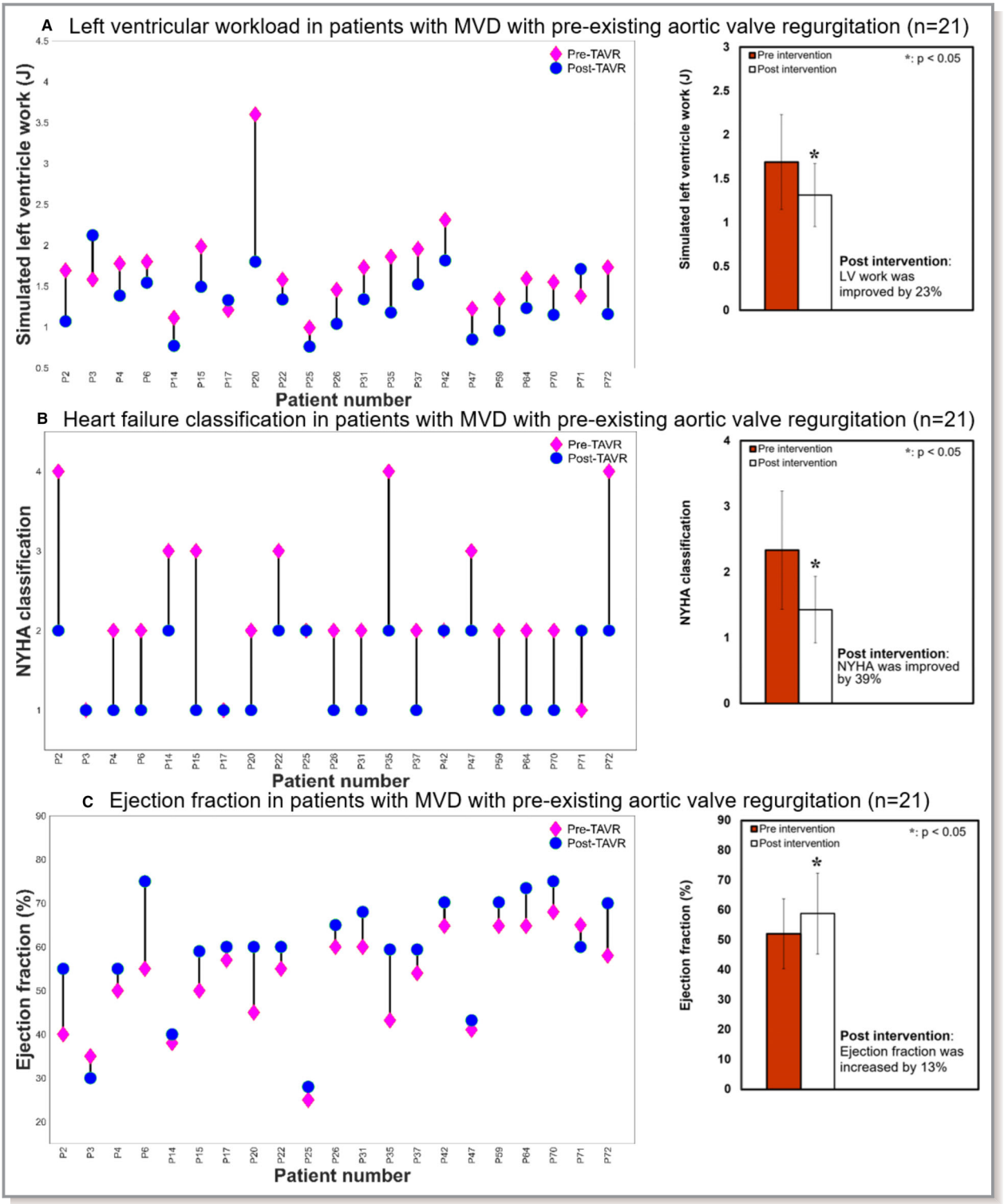

Figure 10. Changes in clinical assessments of LV and LV workloads in patients with MVD with pre-existing aortic valve regurgitation between baseline and 90 days post-TAVR (N=21). (**A**) LV workload. (**B**) Heart failure classification. (**C**) Ejection fraction. LV indicates left ventricle; MVD, mixed valvular diseases; NYHA, New York heart association; TAVR, transcatheter aortic valve replacement.

resistance, which caused an LV pressure overload. Although the flow resistance and consequently the LV pressure decreased greatly postintervention, the LV load did not improve given that PVL contributed to an immediate switching from a LV pressure overload to a LV volume overload (Figures 3 and 4).

Patients With MVD Who Benefited From TAVR

Patients with AS and aortic valve regurgitation, representing up to 40% of the candidates of TAVR, derived great benefits from TAVR despite even developments of a mild PVL post-TAVR that had a minimal influence on outcomes.[32,33] Our results showed that TAVR led to significant improvements in LV workload in MVD patients who had AS and aortic valve regurgitation before the procedure (N=21; Figure 10A). Such LV workload improvements are accompanied by improvements in clinical metrics such as NYHA heart failure classification (Figure 10B) and ejection fraction (Figure 10C).

Patients With PVL Following TAVR, But Without Pre-Existing MR

We investigated 48 patients with post-TAVR PVL, but without pre-existing MR. TAVR reduced LV workload in 28 of these 48 patients (60%; $P<0.05$). In 8 of these patients, LV workload did not significantly reduce (<5% reduction) post-TAVR, and in 12 others, LV workload increased post-TAVR. Indeed, post-TAVR, LV pressure decreased, but LV workload did not always improve because PVL contributed to a switch from LV pressure overload to LV volume overload. The same process happened in patients with MVD, but more intensively. In fact, PVL and MR had mechanical interactions with each other and potentially may contribute in worsening of MR. Most patients who suffered from MVD post-TAVR (75% of N=72; $P<0.05$) showed no improvements or even worsening of LV workload, whereas the majority of the patients with PVL, but without a pre-existing MR condition (60% of N=48; $P<0.05$), showed improvements in LV workload.

Limitations

This study was performed on 72 patients with MVD in both pre- and postintervention states. Future studies must be conducted on a larger population of MVD patients to further confirm the findings of this study. In addition, this study did not consider data collection immediately post-TAVR. Future studies should be designed to include this in the data collection protocol. One limitation that may be associated with our simulations is modeling the transcatheter aortic valve leaflets to be rigidly close and mitral valve leaflets to be rigidly open throughout the diastolic phase. However, this study focuses on diastole, the left ventricular filling phase, when PVL occurs. Furthermore, the good agreement between the numerical simulations (in progress for our other study) and Doppler echocardiography velocity measurements, which include moving valve leaflets, shows that this limitation does not affect the conclusions of this study. Future numerical studies will consider the interactions between the fluid and deforming valve-leaflet structure during the entire cardiac cycle and will investigate the effects of dynamical opening and closing of the aortic valve leaflets on vortex dynamics in the LV.

Conclusions

PVL limits the benefit of TAVR; it may increase LV load, may potentially worsen MR, and worsens heart failure. MR and its possible exacerbation by PVL will likely play an important hindering role in the success of TAVR. This presents an important finding, especially considering the expansion of TAVR candidacy to lower-risk and/or young patients.

The findings of this study suggest that beyond standard clinical indices for hemodynamic evaluation of valvular disease (eg, Doppler echocardiography pressure gradients), valvular and ventricular hemodynamics and their interactions should be clinically quantified and considered to better conduct aortic valve management, treatment planning, and patient risk stratification.

Sources of Funding

Keshavarz-Motamed and Khodaei were supported, in part, by Natural Sciences and Engineering Research Council (NSERC) Discovery Grant (RGPIN-2017-05349). Edelman was supported, in part, by a grant from the National Institutes of Health (GM R01 49039).

Disclosures

Keshavarz-Motamed has research grants from NSERC, but there is no overlap with the work in this study. Edelman has research grants from Edwards LifeSciences, Boston Scientific, and Medtronic, but there is no overlap with the work in this study. The remaining authors have no disclosures to report.

References

1. Padala M, Sarin EL, Willis P, Babaliaros V, Block P, Guyton RA, Thourani VH. An engineering review of transcatheter aortic valve technologies. *Cardiovasc Eng Technol*. 2010;1:77–87.
2. Cortés C, Amat-Santos IJ, Nombela-Franco L, Muñoz-Garcia AJ, Gutiérrez-Ibanes E, De La Torre Hernandez JM, Córdoba-Soriano JG, Jimenez-Quevedo P, Hernández-García JM, Gonzalez-Mansilla A, Ruano J, Jimenez-Mazuecos J, Castrodeza J, Tobar J, Islas F, Revilla A, Puri R, Puerto A, Gómez I, Rodés-Cabau J, San Román JA. Mitral regurgitation after transcatheter aortic valve replacement: prognosis, imaging predictors, and potential management. *JACC Cardiovasc Interv*. 2016;9:1603–1614.
3. Elmariah S, Palacios IF, McAndrew T, Hueter I, Inglessis I, Baker JN, Kodali S, Leon MB, Svensson L, Pibarot P, Douglas PS, Fearon WF, Kirtane AJ, Maniar HS, Passeri JJ; PARTNER Investigators. Outcomes of transcatheter and surgical aortic valve replacement in high-risk patients with aortic stenosis and left ventricular dysfunction results from the Placement of Aortic Transcatheter Valves (PARTNER) trial (cohort A). *Circ Cardiovasc Interv*. 2013;6:604–614.
4. Walsh JA, Teirstein PS, Stinis C, Price MJ. Risk assessment in patient selection for transcatheter aortic valve replacement. *Interv Cardiol Clin*. 2015;4:1–12.
5. Abdel-Wahab M, Zahn R, Horack M, Gerckens U, Schuler G, Sievert H, Eggebrecht H, Senges J, Richardt G; German transcatheter aortic valve interventions registry investigators. Aortic regurgitation after transcatheter aortic valve implantation: incidence and early outcome. Results from the German transcatheter aortic valve interventions registry. *Heart*. 2011;97:899–906.
6. Pibarot P, Hahn RT, Weissman NJ, Monaghan MJ. Assessment of paravalvular regurgitation following TAVR: a proposal of unifying grading scheme. *JACC Cardiovasc Imaging*. 2015;8:340–360.

7. Pibarot P. Paravalvular regurgitation following transcatheter aortic valve replacement: is it still an issue in 2018? *Struct Heart*. 2019;3:31–33.
8. Sannino A, Stoler RC, Vallabhan R, Potluri S, Pollock B, Filardo G, Mack MJ, Grayburn PA. Assessment of the severity of paravalvular regurgitation and its role on survival after transcatheter aortic valve replacement. *Struct Heart*. 2019;3:24–30.
9. Ong G, Annabi MS, Clavel MA, Guzzetti E, Salaun E, Toubal O, Dahou A, Pibarot P. Paravalvular regurgitation after transcatheter aortic valve replacement: is the problem solved? *Interv Cardiol Clin*. 2018;7:445–458.
10. Chiche O, Rodés-Cabau J, Campelo-Parada F, Freitas-Ferraz AB, Regueiro A, Chamandi C, Rodriguez-Gabella T, Côté M, DeLarochellière R, Paradis J-M, Dumont E, Doyle D, Mohammadi S, Bergeron S, Pibarot P, Beaudoin J. Significant mitral regurgitation in patients undergoing TAVR: mechanisms and imaging variables associated with improvement. *Echocardiography*. 2019;36:722–731.
11. Shibayama K, Harada K, Berdejo J, Mihara H, Tanaka J, Gurudevan SV, Siegel R, Jilaihawi H, Makkar RR, Shiota T. Effect of transcatheter aortic valve replacement on the mitral valve apparatus and mitral regurgitation: real-time three-dimensional transesophageal echocardiography study. *Circ Cardiovasc Imaging*. 2014;7:344–351.
12. O'Sullivan CJ, Tüller D, Zbinden R, Eberli FR. Impact of mitral regurgitation on clinical outcomes after transcatheter aortic valve implantation. *Interv Cardiol*. 2016;11:54–58.
13. Pibarot P, Hahn RT, Weissman NJ, Arsenault M, Beaudoin J, Bernier M, Dahou A, Khalique OK, Asch FM, Toubal O, Leipsic J, Blanke P, Zhang F, Parvataneni R, Alu M, Herrmann H, Makkar R, Mack M, Smalling R, Leon M, Thourani VH, Kodali S. Association of paravalvular regurgitation with 1-year outcomes after transcatheter aortic valve replacement with the SAPIEN 3 valve. *JAMA Cardiol*. 2017;2:1208–1216.
14. Zoghbi WA, Asch FM, Bruce C, Gillam LD, Grayburn PA, Hahn RT, Inglessis I, Islam AM, Lerakis S, Little SH, Siegel RJ, Skubas N, Slesnick TC, Stewart WJ, Thavendiranathan P, Weissman NJ, Yasukochi S, Zimmerman KG. Guidelines for the evaluation of valvular regurgitation after percutaneous valve repair or replacement: a report from the American Society of Echocardiography Developed in Collaboration with the Society for Cardiovascular Angiography and Interventions, Japanese Society of Echocardiography, and Society for Cardiovascular Magnetic Resonance. *J Am Soc Echocardiogr*. 2019;32:431–475.
15. Kodali S, Pibarot P, Douglas PS, Williams M, Xu K, Thourani V, Rihal CS, Zajarias A, Doshi D, Davidson M, Tuzcu EM, Stewart W, Weissman NJ, Svensson L, Greason K, Maniar H, Mack M, Anwaruddin S, Leon MB, Hahn RT. Paravalvular regurgitation after transcatheter aortic valve replacement with the Edwards sapien valve in the PARTNER trial: characterizing patients and impact on outcomes. *Eur Heart J*. 2015;36:449–456.
16. Richter Y, Edelman ER. Cardiology is flow. *Circulation*. 2006;113:2679–2682.
17. Nichols W, O'Rourke M, Vlachopoulos C. *McDonald's Blood Flow in Arteries: Theoretical, Experimental and Clinical Principles*. Boca Raton, FL : CRC Press; 2011.
18. Dweck MR, Boon NA, Newby DE. Calcific aortic stenosis: a disease of the valve and the myocardium. *J Am Coll Cardiol*. 2012;60:1854–1863.
19. Otto CM. Valvular aortic stenosis. Disease severity and timing of intervention. *J Am Coll Cardiol*. 2006;47:2141–2151.
20. Pibarot P, Dumesnil JG. Improving assessment of aortic stenosis. *J Am Coll Cardiol*. 2012;60:169–180.
21. Pibarot P, Dumesnil JG. Assessment of aortic stenosis severity: check the valve but don't forget the arteries! *Heart*. 2007;93:780–782.
22. Ben-Assa E, Brown J, Keshavarz-Motamed Z, de la Torre Hernandez JM, Leiden B, Olender M, Kallel F, Palacios IF, Inglessis I, Passeri JJ, Shah PB, Elmariah S, Leon MB, Edelman ER. Ventricular stroke work and vascular impedance refine the characterization of patients with aortic stenosis. *Sci Transl Med*. 2019;11:eaaw0181.
23. Keshavarz-Motamed Z, Rikhtegar Nezami F, Partida RA, Nakamura K, Staziaki PV, Ben-Assa E, Ghoshhajra B, Bhatt BA, Edelman ER. Elimination of transcoarctation pressure gradients has no impact on left ventricular function or aortic shear stress post intervention in patients with mild coarctation. *JACC Cardiovasc Interv*. 2016;9:1953–1965.
24. Keshavarz-Motamed Z, Garcia J, Pibarot P, Larose E, Kadem L. Modeling the impact of concomitant aortic stenosis and coarctation of the aorta on left ventricular workload. *J Biomech*. 2011;44:2817–2825.
25. Keshavarz-Motamed Z, Garcia J, Gaillard E, Capoulade R, Ven FL, Cloutier G, Kadem L, Pibarot P. Non-invasive determination of left ventricular workload in patients with aortic stenosis using magnetic resonance imaging and Doppler echocardiography. *PLoS One*. 2014;9:e86793.
26. Benevento E, Djebbari A, Keshavarz-Motamed Z, Cecere R, Kadem L. Hemodynamic changes following aortic valve bypass: a mathematical approach. *PLoS One*. 2015;10:e0123000.
27. Bedogni F, Latib A, De Marco F, Agnifili M, Oreglia J, Pizzocri S, Latini RA, Lanotte S, Petronio AS, De Carlo M, Ettori F, Fiorina C, Poli A, Cirri S, De Servi S, Ramondo A, Tarantini G, Marzocchi A, Fiorilli R, Klugmann S, Ussia GP, Tamburino C, Maisano F, Brambilla N, Colombo A, Testa L. Interplay between mitral regurgitation and transcatheter aortic valve replacement with the CoreValve Revalving System: a multicenter registry. *Circulation*. 2013;128:2145–2153.
28. Toggweiler S, Boone RH, Rodés-Cabau J, Humphries KH, Lee M, Nombela-Franco L, Bagur R, Willson AB, Binder RK, Gurvitch R, Grewal J, Moss R, Munt B, Thompson CR, Freeman M, Ye J, Cheung A, Dumont E, Wood DA, Webb JG. Transcatheter aortic valve replacement: outcomes of patients with moderate or severe mitral regurgitation. *J Am Coll Cardiol*. 2012;59:2068–2074.
29. Nombela-Franco L, Ribeiro HB, Urena M, Allende R, Amat-Santos I, DeLarochellière R, Dumont E, Doyle D, DeLarochellière H, Laflamme J, Laflamme L, García E, Macaya C, Jiménez-Quevedo P, Côté M, Bergeron S, Beaudoin J, Pibarot P, Rodés-Cabau J. Significant mitral regurgitation left untreated at the time of aortic valve replacement: a comprehensive review of a frequent entity in the transcatheter aortic valve replacement era. *J Am Coll Cardiol*. 2014;63:2643–2658.
30. Gharib M, Rambod E, Kheradvar A, Sahn DJ, Dabiri JO. Optimal vortex formation as an index of cardiac health. *Proc Natl Acad Sci USA*. 2006;103:6305–6308.
31. Burkhoff D, Mirsky I, Suga H. Assessment of systolic and diastolic ventricular properties via pressure-volume analysis: a guide for clinical, translational, and basic researchers. *Am J Physiol Heart Circ Physiol*. 2005;289:H501–H512.
32. Chieffo A, Van Mieghem NM, Tchetche D, Dumonteil N, Giustino G, Van der Boon RMA, Pierri A, Marcheix B, Misuraca L, Serruys PW, Millischer D, Carrié D, de Jaegere PPT, Colombo A. Impact of mixed aortic valve stenosis on VARC-2 outcomes and postprocedural aortic regurgitation in patients undergoing transcatheter aortic valve implantation: results from the International Multicentric Study PRAGMATIC (Pooled Rotterdam-Milan-Toulouse in Collaboration). *Catheter Cardiovasc Interv*. 2015;86:875–885.
33. Van Belle E, Juthier F, Susen S, Vincentelli A, Iung B, Dallongeville J, Eltchaninoff H, Laskar M, Leprince P, Lievre M, Banfi C, Auffray J-L, Delhaye C, Donzeau-Gouge P, Chevreul K, Fajadet J, Leguerrier A, Prat A, Gilard M, Teiger E; FRANCE 2 Investigators. Postprocedural aortic regurgitation in balloon-expandable and self-expandable transcatheter aortic valve replacement procedures: analysis of predictors and impact on long-term mortality: insights from the FRANCE2 registry. *Circulation*. 2014;129:1415–1427.

Supplemental Material

Data S1.

A. Lumped parameter model

The lumped-parameter model (LPM) framework includes the following sub-models: 1) LV; 2) aortic valve; 3) aortic regurgitation and 4) systemic circulation (Figure 1, Tables 1 and 2). All input parameters were obtained from Doppler echocardiography measurements and brachial pressures in both pre and post intervention states. The model and sub-models have already been used and validated against *in vivo* cardiac catheterization (N=113) and *in vivo* MRI data (N=57) [1–6].

Heart-arterial model

The ventricle was filled by a normalized physiological mitral flow waveform adjusted for the required stroke volume. Coupling between left ventricle pressure and volume was performed through a time varying elastance E(t), a measure of cardiac muscle stiffness.

$$E(t) = \frac{P_{LV}(t)}{V(t) - V_0} \quad (1)$$

Where $P_{LV}(t)$, $V(t)$ and V_0 are left ventricular time-varying pressure, time-varying volume and unloaded volume, respectively. The amplitude of E(t) can be normalized with respect to maximal elastance E_{max}, *i.e.*, the slope of the end-systolic pressure-volume relation, giving $E_N(t_N)=E(t)/E_{max}$. Time then can be normalized with respect to the time to reach peak elastance, T_{Emax} ($t_N=t/T_{Emax}$).

$$E_{\max} E_N(t / T_{E\max}) = \frac{P_{LV}(t)}{V(t) - V_0} \quad (2)$$

As normalized curve of $E_N(t_N)$ can be described using Fourier series, therefore, the relation between $P_{LV}(t)$ and $V(t)$ can be determined for the left ventricle.

Modeling aortic valve

Aortic stenosis (AS) was modeled using Equation 3. This formulation expresses the instantaneous net pressure gradient across the stenotic valve (after pressure recovery) as a function of the instantaneous flow rate and the energy loss coefficient and links the LV pressure to the aorta pressure:

$$TPG_{net}\big|_{AS} = P_{LV}(t) - P_A(t) = \frac{2\pi\rho}{\sqrt{E_L Co\big|_{AS}}}\frac{\partial Q(t)}{\partial t} + \frac{\rho}{2E_L Co\big|_{AS}^2}Q^2(t) \quad (3)$$

and

$$E_L Co\big|_{AS} = \frac{(EOA\big|_{COA})A}{A - EOA\big|_{AS}} \quad (4)$$

where $E_L Co\big|_{AS}$, $EOA\big|_{AS}$, A, ρ and Q are the valvular energy loss coefficient, the effective orifice area, ascending aorta cross sectional area, the fluid density and the transvalvular flow rate, respectively. Variable aortic valve resistance (R_{av}) and constant aortic valve inductance (L_{av}) in the LPM are $\frac{\rho}{2E_L Co\big|_{AS}^2}Q(t)$ and $\frac{2\pi\rho}{\sqrt{E_L Co\big|_{AS}}}$, respectively.

Modeling aortic valve regurgitation

Aortic regurgitation (AR) was modeled using the same formulation as aortic stenosis. AR pressure gradient is the difference between aortic pressure and LV pressure during diastole.

$$TPG_{net}\big|_{AR} = \frac{2\pi\rho}{\sqrt{E_L Co\big|_{AR}}}\frac{\partial Q(t)}{\partial t} + \frac{\rho}{2E_L Co\big|_{AR}^2}Q^2(t) \quad (5)$$

and

$$E_L Co\big|_{AR} = \frac{(REOA)A_{LVOT}}{A_{LVOT} - REOA} \quad (6)$$

where $E_L Co|_{AR}$, $REOA$ and A_{LVOT} are regurgitation energy loss coefficient, regurgitant effective orifice area and LVOT area, respectively. Variable aortic valve regurgitation resistance (R_{av}) and constant aortic valve regurgitation inductance (L_{av}) in model are $\frac{\rho}{2E_L Co|_{AR}^2} Q(t)$ and $\frac{2\pi\rho}{\sqrt{E_L Co|_{AR}}}$, respectively.

Determining arterial compliance and peripheral resistance

The total systemic resistance was computed as the quotient of the average brachial pressure and the cardiac output (assuming a negligible peripheral venous pressure (mean ~ 5 mmHg) compared to aortic pressure (mean ~ 100 mmHg). This total systemic resistance represents the electrical equivalent resistance for all resistances in the current model. Because what the left ventricle faces is the total systemic resistance and not the individual resistances, for the sake of simplicity we considered the aortic resistance, R_{ao}, and systemic vein resistance, R_{SV}, as constants and adjusted the systemic artery resistance, R_{SA}, according to the obtained total systemic resistance.

For each degree of hypertension, we fit the predicted pulse pressure to the actual pulse pressure (known by arm cuff sphygmomanometer) obtained from clinical study by adjusting compliances (aorta (C_{ao}) and systemic (C_{SAC})).

Computational algorithm

The lumped parameter model was analyzed numerically by creating and solving a system of ordinary differential equations in Matlab Simscape (MathWorks, Inc.), enhanced by adding additional codes to meet demands of cardiac model in circuit. A Fourier series representation of an experimental normalized elastance curve for human adults was used to generate a signal to be fed into the main program (1,2,3,4). Simulations start at the onset of isovolumic contraction. Left ventricle volume, V(t), is calculated using left ventricle pressure, P_{LV}, and time varying elastance values (equation 1). Matlab's ode23t trapezoidal

rule variable-step solver was used to solve system of differential equations with initial time step of 0.1 milliseconds. The convergence residual criterion was set to 10^{-5} and initial voltages and currents of capacitors and inductors set to zero.

B. Computational fluid mechanics model

In this study, blood flow simulations rely on three dimensions fluid-solid interaction (FSI) computational fluid dynamics using FOAM-Extend [7] in which the system of equations governing the FSI problem are formulated using the finite volume method.

Governing equations for fluid domain

Blood flow was governed by the 3D incompressible Navier-Stokes equations and assumed to be a Newtonian and incompressible with a dynamic viscosity of 0.004 Pa·s and a density of 1060 kg/m^3 [8]. Continuity and momentum equations were as the following:

$$\iint_s (n.v)ds = 0 \tag{7}$$

$$\int_\forall \frac{\partial v}{\partial t} d\forall + \iint_s v[n.v]ds = \frac{1}{\rho}\iint_s n.[\mu \nabla v]ds - \frac{1}{\rho}\int_\forall \nabla p d\forall \tag{8}$$

where n is the normal vector to the surface S, V is the fluid velocity, μ is the fluid dynamic viscosity, P is the blood pressure and ρ is the fluid density. Due to the moving boundary of the fluid-solid interface, momentum equation (8) was considered in the form of Arbitrary Lagrangian-Eulerian (ALE) as follows:

$$\int_\forall \frac{\partial V}{\partial t} d\forall + \iint_s n.(v - v_s)vds = \frac{1}{\rho}\iint_s n.[\mu \nabla v]ds - \frac{1}{\rho}\int_\forall \nabla p d\forall \tag{9}$$

$$\frac{d}{dt}\int_\forall d\forall = \iint_s n.v_s ds \tag{10}$$

where V_s is the velocity of surface. Equation (10) indicates that the rate of changes of the volume and velocity of surface are in equilibrium.

Governing equations for solid domain

Because during diastole, the LV is passive its deformation depends on the tissue structure and the blood pressure inside the LV [9]. In this study, we developed a method to adjust patient-specific passive material properties of the LV for patients who undergo TAVR, based on our patient-specific DE-based LPM algorithm [1–6]. LV tissue was assumed to be an isotropic Saint Venant-Kirchhoff solid [10–15]. We adjusted the ventricular non-linear material properties during diastole using the results of our LPM algorithm as follows. The LPM algorithm provided the diastolic pressure as well as the pressure-volume (P-V) diagram. We applied the diastolic pressure as the boundary condition at the inner wall of the LV and by assuming different values for material properties, we obtained a series of P-V diagrams. Material properties were then interpolated to find the best value that can match the P-V results obtained using solid modeling to those obtained using the LPM.

According to the linear momentum conservation law in the total Lagrangian form, deformation of elastic and compressible solid were considered as the following:

$$\int_{V_0} \rho_0 \frac{\partial}{\partial t}\left(\frac{\partial u}{\partial t}\right) dV = \left[\iint_{s_0} n.(\Sigma.F^T) ds + \int_{V_0} \rho_0 b dV \right. \tag{11}$$

where the subscript 0 describes the undeformed configuration and u is the displacement vector. F is the deformation gradient tensor and can be described as:

$$F = I + (\nabla u)^T \tag{12}$$

where I is the second order Identity tensor. Also, Σ in eq. (11) is the second Piola-Kirchhoff stress tensor and was described through Cauchy stress tensor (σ) as the following:

$$\sigma = \frac{1}{\det F} F.\Sigma.F^T \tag{13}$$

Using St. Venant-Kirchhoff constitutive material model, Σ was explained through isotropic Hooke's law:

$$\Sigma = 2\mu E + \lambda tr(E)I \tag{14}$$

where μ and λ are the Lame's constants (related to the Young's modulus and Poisson's ratio of material). E is the Green-Lagrangian strain tensor and is defined as follows:

$$E = \frac{1}{2}[\nabla u + (\nabla u)^T + \nabla u.(\nabla u)^T] \tag{15}$$

Fluid-structure interaction (FSI)

The fluid and solid solvers were coupled together to simulate the LV under pathophysiological flow and pressure conditions. Both solid and fluid were modeled using finite-volume approach. Fluid and solid solvers were coupled by kinematic and dynamic conditions for the LV. To satisfy the kinematic condition, the velocity and the displacement must be continuous across the interface [7]:

$$u_{f,i} = u_{s,i} \tag{16}$$

$$V_{f,i} = V_{s,i} \tag{17}$$

where subscripts i, s and f indicate the interface, solid and fluid regions, respectively. To satisfy the dynamic condition, the forces at the interface must be in equilibrium:

$$n_i.\sigma_{f,i} = n_i.\sigma_{s,i} \tag{18}$$

The Dirichlet-Neumann procedure at the interface indicates that fluid domain is solved for a given velocity/displacement and solid is solved for a given traction [7].

Boundary conditions & material properties

We used our patient-specific LPM (Figure 1) [1–5] : (1) to provide the time-dependent trans-mitral blood velocity; (2) to set the pressure, inside the LV; (3) to calculate material properties (see section Governing equations for solid domain). All geometries were reconstructed based on images at the beginning of diastole and, because PVL occurs in the left ventricular filling phase, all simulations were performed during diastole. Therefore, the TAVR was modeled to be rigidly closed and the mitral valve was modeled fully opened during the diastolic phase. The boundary surfaces between the fluid and solid inside the LV was considered as Moving wall boundary condition [15,16]. During diastole, there is an inflow from the atrium to the LV but there is no outflow from the LV due to the closed aortic valve. Since the blood is incompressible, interactions between the solid and fluid domains should be considered to allow the blood to expand and contract the LV wall to conserve mass. In order to solve the FSI problem inside the nonlinearly deforming LV, we used the Robin boundary condition for pressure based on the approach proposed by Tukovic et al [17].

Reconstructed geometries in patients with TAVR using CT images

We used CT images from patients with TAVR to segment and reconstruct the 3D geometries of the complete ventricle (ventricle, TAVR, coronaries, mitral valve and left atrium) using ITK-SNAP (version 3.8.0-BETA), a 3D image processing and model generation software package (Figure 1). These 3-D reconstructions were used for investigating hemodynamic using computational fluid dynamics.

Supplemental References:

1. Keshavarz-Motamed Z, Rikhtegar Nezami F, Partida RA, Nakamura K, Staziaki PV, Ben-Assa E, Ghoshhajra B, Bhatt BA, Edelman ER. Elimination of trans-coarctation pressure gradients has no impact on left ventricular function or aortic shear stress post intervention in patients with mild coarctation. *JACC Cardiovasc Interv*. 2016;9:1953–1965.

2. Ben-Assa E, Brown J, Keshavarz-Motamed Z, de la Torre Hernandez JM, Leiden B, Olender M, Kallel F, Palacios IF, Inglessis I, Passeri JJ, Shah PB, Elmariah S, Leon MB, Edelman ER. Ventricular stroke work and vascular impedance refine the characterization of patients with aortic stenosis. *Sci Transl Med*. 2019;11.

3. Keshavarz-Motamed Z, Garcia J, Pibarot P, Larose E, Kadem L. Modeling the impact of concomitant aortic stenosis and coarctation of the aorta on left ventricular workload. *J Biomech*. 2011;44:2817–2825.

4. Keshavarz-Motamed Z, Garcia J, Gaillard E, Capoulade R, Ven FL, Cloutier G, Kadem L, Pibarot P. Non-Invasive Determination of Left Ventricular Workload in Patients with Aortic Stenosis Using Magnetic Resonance Imaging and Doppler Echocardiography. *PLOS ONE*. 2014;9:e86793.

5. Benevento E, Djebbari A, Keshavarz-Motamed Z, Cecere R, Kadem L. Hemodynamic Changes following Aortic Valve Bypass: A Mathematical Approach. *PLOS ONE*. 2015;10:e0123000.

6. K. Motamed Z. A diagnostic, monitoring, and predictive tool for patients with complex valvular, vascular and ventricular diseases. *Nat Sci Rep*. 2019;Under review.

7. Tuković Ž, Karač A, Cardiff P, Jasak H, Ivanković A. OpenFOAM Finite Volume Solver for Fluid-Solid Interaction. *Trans FAMENA*. 2018;42:1–31.

8. Khodaei S, Fatouraee N, Nabaei M. Numerical simulation of mitral valve prolapse considering the effect of left ventricle. *Math Biosci*. 2017;285:75–80.

9. Nikolić S, Yellin EL, Tamura K, Vetter H, Tamura T, Meisner JS, Frater RW. Passive properties of canine left ventricle: diastolic stiffness and restoring forces. *Circ Res*. 1988;62:1210–1222.

10. Bagnoli P, Malagutti N, Gastaldi D, Marcelli E, Lui E, Cercenelli L, Costantino ML, Plicchi G, Fumero R. Computational Finite Element Model of Cardiac Torsion. *Int J Artif Organs*. 2011;34:44–53.

11. Hassaballah AI, Hassan MA, Mardi AN, Hamdi M. An Inverse Finite Element Method for Determining the Tissue Compressibility of Human Left Ventricular Wall during the Cardiac Cycle. *PLOS ONE*. 2013;8:e82703.

12. Hassan MA, Hamdi M, Noma A. The nonlinear elastic and viscoelastic passive properties of left ventricular papillary muscle of a Guinea pig heart. *J Mech Behav Biomed Mater*. 2012;5:99–109.

13. Quaini A, Canic S, Glowinski R, Igo S, Hartley CJ, Zoghbi W, Little S. Validation of a 3D computational fluid–structure interaction model simulating flow through an elastic aperture. *J Biomech*. 2012;45:310–318.

14. Topnes E. Computational modelling of cardiac mechanics - Efficient simulation of a heartbeat. *83*. 2016.

15. Govindarajan V, Mousel J, Udaykumar HS, Vigmostad SC, McPherson DD, Kim H, Chandran KB. Synergy between Diastolic Mitral Valve Function and Left Ventricular Flow Aids in Valve Closure and Blood Transport during Systole. *Sci Rep*. 2018;8:1–14.

16. Moosavi M-H, Fatouraee N, Katoozian H, Pashaei A, Camara O, Frangi AF. Numerical simulation of blood flow in the left ventricle and aortic sinus using magnetic resonance imaging and computational fluid dynamics. *Comput Methods Biomech Biomed Engin*. 2014;17:740–749.

17. Tuković Ž, Bukač M, Cardiff P, Jasak H, Ivanković A. Added Mass Partitioned Fluid–Structure Interaction Solver Based on a Robin Boundary Condition for Pressure. In: Nóbrega JM, Jasak H, eds. OpenFOAM®. Cham: Springer International Publishing; 2019: 1–22.